

IMPULSIVE CONTROL OF FORMATIONS NEAR INVARIANT TORI VIA LOCAL TOROIDAL COORDINATES

Ian Elliott* and Natasha Bosanac†

Invariant tori relative to periodic orbits have historically been identified as a useful reference for locating spacecraft formations in multi-body environments. An impulsive control strategy is presented to enable geometric formations of spacecraft operating near periodic orbits. Toroidal coordinates that represent the relative state of a spacecraft in relation to the center eigenspace of a periodic orbit are used to develop a targeting strategy that is capable of tracking specific deviations from a periodic orbit. The presented strategy is developed using the circular restricted three-body problem and assessed in a point-mass ephemeris model of the Sun-Earth system with perturbations from solar radiation pressure.

INTRODUCTION

Formations of spacecraft in multi-body environments may enable space-based observations of scientific phenomena and reduce the cost of future missions.¹ Previous concepts for distributed space systems in multi-body environments include the Terrestrial Planet Finder,² Stellar Imager,³ and Darwin,⁴ focused on placing formations of spacecraft in multi-body environments to search for potentially habitable planets, study stellar magnetic activity, and achieve other scientific objectives. Trajectories near the Sun-Earth equilibrium points have specifically been identified as favorable locations for spacecraft due to communication geometry, thermal stability, and reasonable station-keeping requirements.^{2,5} Space-based interferometers formed by passive clusters of spacecraft may also observe heliophysics activities such as coronal mass ejections.⁶ This type of passive interferometry does not require active reconfiguration so long as antenna positions are known⁷ and motivates the use of natural motion within formation trajectory design.

An existing strategy for the design of formations in simplified dynamical models of multi-body systems such as the circular restricted three-body problem (CR3BP) places spacecraft on the surface of invariant tori that exist near periodic orbits to achieve bounded relative motion.⁸ However, computation of invariant tori in the nonlinear CR3BP is a computationally expensive numerical process.^{9,10} For small separation distances from a periodic orbit, the local center eigenspace of the periodic orbit supplies a suitable approximation of oscillatory motion corresponding to invariant tori.^{11,12} While the motion along an invariant torus is naturally bounded in the vicinity of a periodic orbit, small deviations may quickly grow in the chaotic dynamical environment.¹³ Because of this sensitivity, control may be necessary to maintain bounded formations.

*Graduate Researcher, Colorado Center for Astrodynamics Research, Smead Aerospace Engineering Sciences, University of Colorado Boulder, Boulder, CO 80303

†Assistant Professor, Colorado Center for Astrodynamics Research, Smead Aerospace Engineering Sciences, University of Colorado Boulder, Boulder, CO 80303

Several strategies for the control of spacecraft near periodic orbits have been introduced that incorporate information on the local eigenspaces of the periodic orbit to determine impulsive maneuvers. Spacecraft control strategies that leverage naturally-bounded relative motion may require lower station-keeping control usage compared to targeting non-natural motion.¹⁴ Floquet mode strategies, as presented by Simo et al.,¹⁵ determine instantaneous maneuvers that periodically eliminate the unstable component of a spacecraft state relative to a periodic orbit. This method was further developed by Howell and Marchand¹⁴ to eliminate both unstable and periodic components to control the motion of spacecraft onto only the stable and center eigenspaces, resulting in bounded oscillatory motion near a periodic orbit. Another impulsive station-keeping strategy, introduced by Pavlak and Howell,¹⁶ uses the direction of the stable eigenspace of a periodic orbit as an initial guess for long-term, optimal station-keeping maneuvers of a single spacecraft near a periodic orbit. Continuous control schemes have also been developed that incorporate insight into the local stability of periodic orbits, including continuous Floquet mode methods,^{17,18} Lyapunov function-based feedback control,¹⁹ and other modal strategies.²⁰ However, impulsive control strategies are the focus of this analysis.

While Floquet control methods are well-suited to stabilizing a single spacecraft relative to a reference periodic orbit, formations of spacecraft near an associated periodic orbit may require stricter constraints, such as formation geometry maintenance and collision-avoidance. These constraints require spacecraft to be capable of tracking specific deviations from a reference periodic orbit. Surveys by Folta²¹ and Shirobokov et al.²² present comprehensive discussions of station-keeping strategies for spacecraft near periodic orbits in the CR3BP, capturing the current state-of-the-art in station-keeping strategies. Targeting methods, such as formulations presented by Howell and Barden¹² and Qi et al.,²³ support tracking of specific deviations from a periodic orbit. Furthermore, target point methods, introduced by Howell and Pernika²⁴ and modified by Howell and Gordon,²⁵ modify the targeting problem into a optimization problem. However, unlike Floquet mode control, these targeting schemes do not require knowledge of the local stability of the periodic orbit. These prior works motivate combining the benefits of both modal and targeting impulsive control strategies for spacecraft near periodic orbits.

To develop an impulsive control strategy that incorporates characteristics of both modal and targeting strategies, a family of local toroidal coordinates introduced by Elliott and Bosanac²⁶ is employed in this analysis. The introduced toroidal coordinates decompose a state relative to a periodic orbit in terms of the projection onto, and deviation from, the center eigenspace and have previously been applied to the derivation of a nonlinear feedback control algorithm for spacecraft near periodic orbits with oscillatory modes.¹⁹ When expressed using local toroidal coordinates, motion in the center eigenspace is time-invariant in the CR3BP when linearized about a periodic orbit. Additionally, the toroidal coordinates possess a geometric interpretation of the amplitude and poloidal angle along a torus, as well as separation of a state from the center eigenspace. This geometric decomposition enables the intuitive definition of the states of multiple spacecraft in a formation, each following distinct references tracing the same approximated invariant torus, corresponding to first-order approximations of quasi-periodic orbits.

In this paper, an impulsive targeting control strategy for spacecraft in a formation near a periodic orbit is formulated using local toroidal coordinates. The strategy modifies existing linear targeting strategies that use a state transition matrix to determine a maneuver that targets a specific deviation from a reference orbit after a specified time. For this strategy, a state transition matrix evaluated along a periodic orbit is reformulated in the toroidal coordinate frame to map between initial and

final deviations defined in toroidal coordinates. Then, leveraging the slow description of motion near the center eigenspace, simplifications are applied to the state transition matrix formulated in the toroidal coordinate frame. The resulting strategy supplies impulsive feedback control that supports tracking distinct deviations from a reference trajectory that lies in the center eigenspace. The strategy combines the benefit of targeting strategies, that is, the ability to target specific deviations, with the benefits of the Floquet mode strategies, which incorporate knowledge of naturally bounded motion relative to a periodic orbit. First, the CR3BP dynamical model is summarized, followed by the description of a point-mass ephemeris model with perturbations from solar radiation pressure (SRP) used in this paper as a higher-fidelity model of spacecraft dynamics. Next, an overview of invariant tori near periodic orbits in the CR3BP is included, as well as a summary of the local toroidal coordinate formulation employed by the control strategy. The derivation of the impulsive control strategy is then detailed. To validate the simplifying assumptions within the derivation, the performance of the strategy is first assessed in the CR3BP. Then, to assess the performance of the strategy in a higher-fidelity dynamical model, a Monte Carlo analysis is conducted that incorporates navigational and thruster firing error models. The required control costs, steady-state error, and overall robustness of the strategy are investigated. Finally, a comprehensive application of the control strategy to a conceptual spacecraft formation near a Sun-Earth L_1 halo orbit is presented. This example serves as a demonstration of the presented strategy to the control of a formation of spacecraft in an environment where previously only single spacecraft have operated.

DYNAMICAL MODELS

The presented control strategy is formulated using insight from dynamical systems theory as applied to the analysis of periodic orbits in the CR3BP and to the control of spacecraft near reference trajectories that exist in a higher-fidelity dynamical model. In this section, a brief overview of the reference frame and equations of motion of the CR3BP is presented. Next, a point-mass ephemeris model with perturbations from SRP is introduced as a higher-fidelity dynamical model for assessing the performance of the control strategy. Finally, the procedure used to recover a reference trajectory in the ephemeris model that possesses similar properties to periodic orbits is briefly summarized. States along this trajectory serve as the formation center, used as a reference for specifying the relative state of one or more chaser spacecraft.

The Circular Restricted Three-Body Problem

The CR3BP is a well-known dynamical model that approximates the motion of spacecraft under the gravitational influence of two celestial bodies, assumed to be point masses that travel in circular orbits about their mutual barycenter.²⁷ The approximated dynamical model provides autonomous equations of motion for a single spacecraft, and admits several fundamental solutions, including equilibrium points, periodic orbits, and quasi-periodic orbits.²⁸ Specifically, this analysis uses the Sun-Earth CR3BP to simulate the motion of spacecraft in the Sun-Earth system.

The equations of motion of the CR3BP are expressed using a rotating frame defined by the two primary bodies. The two primary celestial bodies are denoted P_1 and P_2 , where P_1 is the more massive body. The rotating frame, denoted $R : \{\hat{x}, \hat{y}, \hat{z}\}$, is defined such that \hat{x} is directed from P_1 to P_2 , \hat{z} is aligned with the orbital angular momentum vector of the P_1 - P_2 system, and \hat{y} completes the right-handed, orthogonal coordinate frame. A nondimensionalization scheme is applied such that quantities of length are normalized by the assumed constant distance between P_1 and P_2 , quantities of time are normalized to produce a mean motion of the P_1 - P_2 system equal to unity, and quantities

of mass are normalized by the total mass of the P_1 - P_2 system. Using this nondimensionalization scheme, a mass ratio, μ , is defined as $\mu = m_2/(m_1 + m_2)$, where m_j is the mass of body j . In the Sun-Earth CR3BP, the mass ratio is approximately $\mu = 3.0035 \times 10^{-6}$. Under the assumptions of the CR3BP, the positions of P_1 and P_2 are constant in the rotating frame and equal to the nondimensional vectors $\mathbf{r}_1 = -\mu\hat{\mathbf{x}}$ and $\mathbf{r}_2 = (1 - \mu)\hat{\mathbf{x}}$, respectively. The position vector of P_3 relative to the barycenter, \mathbf{r}_3 , expressed in the rotating frame is defined as $\mathbf{r}_3 = [x, y, z]^T$. Finally, the state of a spacecraft in the CR3BP is expressed in the rotating frame and relative to the inertially-fixed barycenter of the P_1 - P_2 system as $\mathbf{x}_3 = [x, y, z, \dot{x}, \dot{y}, \dot{z}]^T$. Using these definitions, the nondimensional equations of motion of the CR3BP in the rotating frame are written as the following three scalar, second-order differential equations:

$$\ddot{x} = 2\dot{y} + \frac{\partial U^*}{\partial x}, \quad \ddot{y} = -2\dot{x} + \frac{\partial U^*}{\partial y}, \quad \ddot{z} = \frac{\partial U^*}{\partial z} \quad (1)$$

where U^* is a pseudo-potential function, defined as $U^* = (x^2 + y^2)/2 + (1 - \mu)/r_{13} + \mu/r_{23}$ and the position vectors, r_{13} and r_{23} , are the magnitudes of the relative position vectors for P_3 from P_1 and P_2 , respectively. Throughout this paper, relative position vectors are defined as $\mathbf{r}_{kj} = \mathbf{r}_j - \mathbf{r}_k$. In this formulation, the equations of motion of the spacecraft are autonomous and facilitate a dynamical systems theory analysis of solutions in the approximated model.

Point-Mass Ephemeris Model with SRP

A point-mass ephemeris model of the Sun, Earth, and Moon is used to model spacecraft motion in higher fidelity. The Sun, Earth, and Moon are modeled as point masses and their paths are defined using the NASA Jet Propulsion Laboratory DE421 ephemerides, accessed via the SPICE toolkit.²⁹ This higher fidelity model also include the accelerations due to SRP acting on spacecraft, approximated using a spherical model.³⁰ Selecting the Earth as the primary body with third-body effects from the Sun and the Moon, and perturbations from SRP, the total inertial acceleration of a spacecraft, denoted by the subscript s , relative to the Earth is expressed as^{30,31}

$$\ddot{\mathbf{r}}_{E,sc} = -Gm_E \frac{\mathbf{r}_{E,sc}}{r_{E,sc}^3} + \sum_{j=M,S}^N Gm_j \left(\frac{\mathbf{r}_{sc,j}}{r_{sc,j}^3} - \frac{\mathbf{r}_{E,j}}{r_{E,j}^3} \right) + C_R P_S r_{AU}^2 \frac{A}{m} \frac{\mathbf{r}_{S,sc}}{r_{S,sc}^3} \quad (2)$$

where subscripts E , S , and M correspond to the Earth, Sun, and Moon, respectively. The approximate SRP model requires the following quantities: the solar flux at 1 AU, P_R ; the reflectivity coefficient of the spacecraft, C_R ; the surface-area-to-mass ratio of the spacecraft, A/m ; and the mean distance from the Sun to the Earth, r_{AU} . The mass of each spacecraft is assumed to remain constant throughout this analysis. The SRP and gravitational parameters, Gm , values are consistent with NASA Goddard Space Flight Center's General Mission Analysis Tool.³² In implementation, the state of a spacecraft in this dynamical model is expressed and integrated in the Geocentric Celestial Reference Frame (GCRF).³¹ Throughout this paper, this dynamical model is referred to as the ephemeris model for brevity.

In this paper, it is assumed that the motion of all chaser spacecraft and the formation center are governed by the ephemeris model with the same SRP properties. In a previous investigation by Farres et al.,^{33,34} the authors identify the challenges posed by differential SRP near Sun-Earth equilibrium points, which may result in a chaser spacecraft using propellant to mitigate the natural acceleration differences between spacecraft in a formation due to SRP in order for spacecraft

to remain in close proximity to each other. For this analysis, each spacecraft, including the non-physical formation center, are assumed to have the same physical characteristics affecting the SRP perturbation, that is, the same area-to-mass ratio and reflectivity coefficient. A reflectivity coefficient of $C_R = 1.8$ and a surface-area-to-mass ratio of $A/m = 0.01 \text{ m}^2/\text{kg}$ are selected to represent the characteristics of a small satellite.³⁵ Future investigation may analyze the effects of different area-to-mass ratios or differential SRP between spacecraft on the presented control strategy.

Spacecraft Formation Reference Trajectory in the Ephemeris Model

The reference trajectory used as the formation center in the ephemeris model is assumed to share similar geometric characteristics with a periodic orbit in the CR3BP, and is computed via a numerical corrections scheme. Following the process presented by Pavlak,³⁶ a multiple-shooting scheme is used to recover a continuous trajectory in the ephemeris model using a periodic orbit in the CR3BP as an initial guess. First, several revolutions of a periodic orbit are discretized into multiple arcs. The initial state of each arc is then transformed into the GCRF frame using the instantaneous states of the Sun and Earth from the SPICE ephemerides. A free variable and constraint formulation is used to constrain state and epoch continuity across the trajectory in the ephemeris model. Specifically, the free variable vector is constructed to contain the initial state, initial epoch, and integration time of each arc. The constraint vector is formulated to enforce continuity in the full state and epoch between the end of each arc and the beginning of the following arc. The initial epoch of the trajectory is also constrained to a desired value. Using a multivariate Newton's method, the free variables are updated iteratively until the constraints are satisfied to within a sufficient numerical tolerance, and a continuous trajectory in the ephemeris model is recovered. Within the numerical corrections process, nondimensionalized quantities are used to prevent ill-conditioning of the partial derivative matrix used within the multivariate Newton's method.

In this paper, the reference trajectory in the ephemeris model lies close to a Sun-Earth L_1 southern halo in the CR3BP. The selected periodic orbit possesses a nondimensional state at apogee of approximately $\mathbf{x} = [0.98888, 0, -0.00081065, 0, 0.0089041, 0]^T$ and a period of approximately $T = 177.84$ days in the CR3BP. A continuous reference trajectory is recovered in the ephemeris model using this periodic orbit and the previously outlined scheme with an initial desired epoch on January 1, 2025. The recovered trajectory is displayed in Figure 1 in the Sun-Earth rotating frame with the orbit of the Moon over the same time duration plotted for reference. The trajectories are plotted relative to the Earth, which is fixed as the origin of the rotating coordinate system. The trajectory has an average positive out-of-plane amplitude of approximately 1.483×10^5 km. This reference trajectory is similar to the orbit of International Sun-Earth Explorer-3 (ISEE-3) and Solar and Heliospheric Observatory (SOHO),³⁷ and is used in the following sections to demonstrate the presented control strategy.

INVARIANT TORI NEAR PERIODIC ORBITS IN THE CR3BP

The presented control strategy is designed for the control of one or more chaser spacecraft leveraging naturally-bounded relative motion near either a periodic orbit in the CR3BP or a reference trajectory in the ephemeris model with similar geometric characteristics to a periodic orbit. In this section, a brief description of the stability analysis of periodic orbits in the CR3BP is presented. Next, the local toroidal coordinate systems introduced by Elliott and Bosanac are summarized, including the coordinate transformation between the toroidal coordinate frame and the rotating frame. Examples of first-order approximations of invariant tori near Sun-Earth L_1 and L_2 halo orbits that

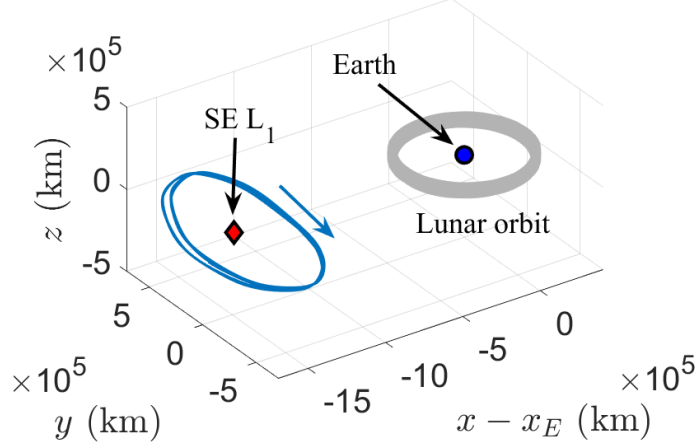


Figure 1. Reference trajectory in the ephemeris model with similar characteristics to a Sun-Earth southern L_1 halo orbit.

admit nearby quasi-periodic relative motion are then presented. Finally, a process for approximating the center eigenspace of a periodic orbit in the ephemeris model is discussed.

Approximating Invariant Tori Near Periodic Orbits

While invariant tori have been previously investigated as a structure for the design of naturally bounded spacecraft motion near periodic orbits, first-order approximations of invariant tori have been demonstrated to be useful for spacecraft formation flying scenarios.^{11,14} To construct a first-order approximation of an invariant torus near a periodic orbit, the stability characteristics of a periodic orbit in the CR3BP are first assessed. Because periodic orbits in the CR3BP exhibit periodicity in the rotating frame, Floquet Theory may be applied.²⁸ A State Transition Matrix (STM) along the periodic orbit between an initial time, t_0 , to a final time, t , is denoted as, $\Phi(t, t_0)$. Using the Jacobian, A , of the CR3BP equations of motion, an STM is calculated via numerical integration of the differential equation $d\Phi(t, t_0)/dt = A(t)\Phi(t, t_0)$, with the initial conditions, $\Phi(t_0, t_0) = I_6$.³⁸ The STM evaluated from t_0 for one period, T , of the periodic orbit is denoted as the monodromy matrix, $M(t_0) = \Phi(t_0 + T, t_0)$. The eigenvalues of the monodromy matrix formulated in the rotating frame, λ , describe the local stability of the periodic orbit while the corresponding eigenvectors, $w(t_0)$, describe the span of the local eigenspaces at t_0 .

An invariant torus exists near a periodic orbit in the nonlinear CR3BP with a monodromy matrix that admits a complex-conjugate pair of eigenvalues that lie on the unit circle.³⁸ The corresponding complex eigenvectors span the center eigenspace and are used to develop a first-order approximation of an invariant torus in the CR3BP and relative to the associated periodic orbit. The set of states, φ , that lie on the center eigenspace of the periodic orbit at time t are calculated using the complex eigenvector of the monodromy matrix, $w(t)$, as⁹

$$\varphi(t) = \varepsilon (\text{Re}(w(t)) \cos \theta + \text{Im}(w(t)) \sin \theta) \quad (3)$$

where ε is a positive scaling term and θ is a parameter defined between 0 and 2π . For a single value of ε at a fixed time, the set φ forms a first-order, elliptical approximation of the instantaneous invariant curve of an invariant torus relative to the fixed point along the periodic orbit.²⁶

Constructing a first-order approximation of an invariant torus in the CR3BP requires knowledge of φ over one period of the periodic orbit. When formulated in the rotating frame, the span of the center eigenspace of a periodic orbit is generally time-varying. Using initial conditions of a complex eigenvector of the monodromy matrix at a fixed point along a periodic orbit, $w(t_0)$, the evolution of the eigenvector along the periodic orbit is computed by numerically integrating the vector differential equation $dw(t)/dt = A(t)w(t)$.³⁹ Using the eigenvector information over a period of the orbit, the surface of a first-order approximation of an invariant torus relative to the periodic orbit is constructed by generating the set φ at a discrete number of fixed points along the periodic orbit for a constant value of ε and several values of θ between 0 and 2π .

As an example, first-order approximations of tori near Sun-Earth L_1 and L_2 halo orbits are constructed and visualized. In Figure 2, several low z -amplitude members of the Sun-Earth northern and southern L_1 and L_2 halo orbit families are illustrated in the rotating frame; the Earth is located by a black marker. Members of the northern and southern L_1 halo families are indicated by cyan and magenta, respectively, and members of the northern and southern L_2 halo families are represented by red and blue, respectively. Illustrated at the boundaries of Figure 2 are examples of first-order approximations of invariant tori, visualized relative to their associated periodic orbits in the rotating frame. The surfaces of the tori visualized in Figure 2 possess complex geometries that vary for different associated periodic orbits in the Sun-Earth halo orbit families. Additionally, an infinite number of nested tori exist relative to each periodic orbit. To facilitate the description of this motion within the presented control strategy, local toroidal coordinates that describe motion relative to periodic orbits with oscillatory modes are employed.

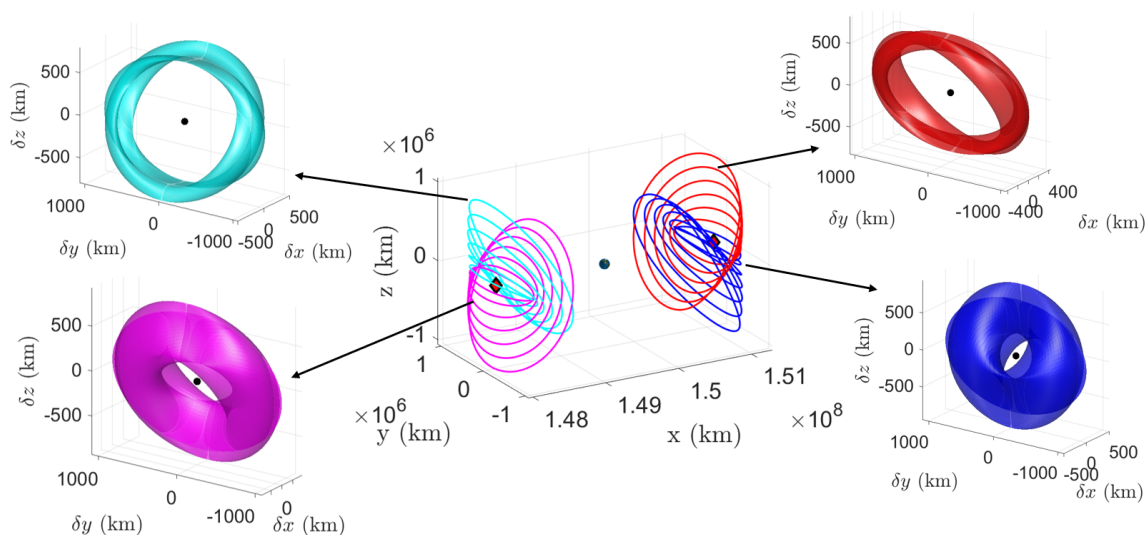


Figure 2. Members of the northern and southern Sun-Earth L_1 and L_2 halo orbit families with selected first-order approximations of invariant tori.

Overview of Local Toroidal Coordinates

The local toroidal coordinate sets introduced by Elliott and Bosanac²⁶ supply useful state representations for spacecraft located near the surfaces of first-order approximations of invariant tori relative to a periodic orbit. Two formulations of local toroidal coordinates are summarized, denoted the nonsingular and the geometric local toroidal coordinates. The state representations decompose

the configuration of a spacecraft relative to a periodic orbit in terms of the projection onto, and separation distance from, the center eigenspace of the orbit. Thus, use of toroidal coordinates is not limited to the description of motion in the center eigenspace. A key property of the toroidal coordinates is that motion along the center eigenspace is described by a two-dimensional, time-invariant set which possess a consistent interpretation across different periodic orbits.

To transform between Cartesian coordinates and local toroidal coordinates, knowledge of the complex eigenvector corresponding to an oscillatory mode of the periodic orbit is required. The complex eigenvector requires a normalization process to remove ambiguity in the definition and ensure consistent results using toroidal coordinates.²⁶ Following the normalization process, a unique complex eigenvector is defined at a selected fixed point along the periodic orbit. The complex eigenvector is decomposed into four, 3×1 vectors corresponding to position and velocity components, denoted by \mathbf{r} and \mathbf{v} , respectively, and real and imaginary components, denoted by subscripts r and i , respectively. The complex eigenvector is then expressed as $\mathbf{w} = [\mathbf{r}_r^T, \mathbf{v}_r^T]^T + i[\mathbf{r}_i^T, \mathbf{v}_i^T]^T$. The position components, \mathbf{r}_r and \mathbf{r}_i , span the plane containing the projection of the center eigenspace onto the configuration space at the selected fixed point. This plane is described by the unit vector, $\hat{\mathbf{n}}$, defined as $\hat{\mathbf{n}} = \mathbf{n}/n$, where $\mathbf{n} = \mathbf{r}_r \times \mathbf{r}_i$. For the implementation detailed in this paper, the complex eigenvector and corresponding components are formulated in the rotating frame.

The toroidal coordinates are local coordinate systems that describe the state of a chaser spacecraft relative to the state of a target spacecraft or reference trajectory following a periodic orbit. The basis vectors of the coordinate system varies over time as the reference travels along the periodic orbit. The relative position, $\boldsymbol{\rho}$, of a chaser spacecraft from a fixed point along the periodic orbit is defined as $\boldsymbol{\rho} = \mathbf{r}_c - \mathbf{r}_t$. Using the rotating frame basis, relative position is expressed as $\boldsymbol{\rho} = \delta x \hat{\mathbf{x}} + \delta y \hat{\mathbf{y}} + \delta z \hat{\mathbf{z}}$. This relative position is equivalently expressed as a linear combination of the position components of the complex eigenvector, \mathbf{r}_r and \mathbf{r}_i , and the normal unit vector $\hat{\mathbf{n}}$, as $\boldsymbol{\rho} = \alpha \mathbf{r}_r + \beta \mathbf{r}_i + h \hat{\mathbf{n}}$. The set of scalar quantities, (α, β, h) , are defined as the nonsingular relative toroidal coordinates, which uniquely describe the configuration of chaser spacecraft relative to a fixed point along a periodic orbit with oscillatory modes. To compute their values, the toroidal coordinates are first defined using the set $\mathbf{z} = [\alpha, \beta, h]^T$. The 3×3 matrix, \mathbf{R} , containing the basis vectors of the toroidal coordinate system in the rotating frame is defined as $\mathbf{R} = [\mathbf{r}_r, \mathbf{r}_i, \hat{\mathbf{n}}]$. Then, the nonsingular relative toroidal coordinates are computed using a linear transformation from the rotating frame, expressed as $\mathbf{z} = \mathbf{R}^{-1} \delta \mathbf{r}$ where $\delta \mathbf{r} = [\delta x, \delta y, \delta z]^T$. A conceptual illustration of the nonsingular toroidal coordinate description of the configuration of a chaser spacecraft relative to a periodic orbit is included in Figure 3(a). The formation center reference trajectory is denoted by t , while the chaser spacecraft is denoted by c .

The three basis vectors of the toroidal coordinate frame and a fixed point along a periodic orbit supply a useful coordinate system for spacecraft motion near the center eigenspace of a periodic orbit. The toroidal frame is denoted as $\mathcal{Z} : \{\mathbf{r}_r, \mathbf{r}_i, \hat{\mathbf{n}}\}$. In general, the basis vectors \mathbf{r}_r and \mathbf{r}_i are non-orthogonal, and the magnitudes of \mathbf{r}_r and \mathbf{r}_i are not equal to one. Thus, units of length are not preserved during the transformation from the rotating frame, and differ from unit of Cartesian position (e.g., kilometers) along the \mathbf{r}_r and \mathbf{r}_i directions. Because these basis vectors evolve along the center manifold, they correspond to quasi-periodic motion. Thus, the matrix \mathbf{R} is not periodic (i.e., $\mathbf{R}(t_0) \neq \mathbf{R}(t_0 + T)$). Furthermore, a curvilinear formulation of local toroidal coordinates, termed geometric relative toroidal coordinates, is used to increase insight into the configuration relative to the center eigenspace. The geometric toroidal coordinates are an alternative to the planar toroidal coordinates, α and β , which describe the projection of the spacecraft on the center eigenspace. The

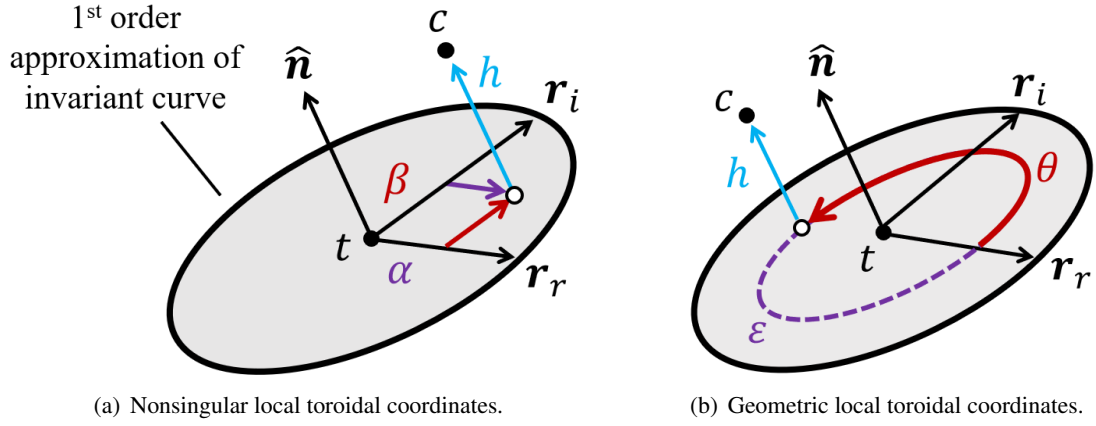


Figure 3. Conceptual illustrations of the local toroidal coordinate sets used to describe motion relative to a periodic orbit with oscillatory modes.

geometric coordinates, ε and θ , are defined via the following nonlinear functions: $\varepsilon = \sqrt{\alpha^2 + \beta^2}$ and $\theta = \tan^{-1}(\beta/\alpha)$. The geometric toroidal coordinates are related to the nonsingular toroidal coordinate as: $\alpha = \varepsilon \cos \theta$ and $\beta = \varepsilon \sin \theta$. The coordinate, ε , describes the size of the torus relative to the periodic orbit, and the coordinate, θ , is an angle parameter indicating rotation along the poloidal direction of the torus.²⁶ The third coordinate, h , is shared with the nonsingular toroidal coordinate set. This local toroidal coordinate set adds geometric insight into the state of a chaser spacecraft, and is conceptually illustrated in Figure 3(b).

The time derivatives of the local toroidal coordinates are useful for understanding the deviation of the state of the chaser spacecraft from motion on the center eigenspace. The time derivative of the nonsingular toroidal coordinates for an observer in the toroidal coordinate frame, ${}^Z z'$, is calculated from the relative velocity for an observer in the rotating frame, $\delta v = [\delta \dot{x}, \delta \dot{y}, \delta \dot{z}]^T$, as

$${}^Z z' = R^{-1} \delta v - R^{-1} R' R^{-1} \delta r \quad (4)$$

When this velocity is expressed in the toroidal coordinate frame, it is equal to ${}^Z z' = [\dot{\alpha}, \dot{\beta}, \dot{h}]^T$. The computation of the coordinate rates expressed in Eq. (4) requires the time derivative of the toroidal coordinate frame basis vectors for an observer in the rotating frame, defined as $R' = [v_r, v_i, \hat{n}']$. The time derivatives of the toroidal coordinates describe the difference between a spacecraft's relative velocity with respect to the periodic orbit, and the velocity of motion on the center eigenspace, such that the time derivatives of the three coordinates are each equal to 0 when a spacecraft lies on the center eigenspace. Thus, using the toroidal coordinates, a state on the center eigenspace is straightforwardly designed by selecting $h = \dot{\alpha} = \dot{\beta} = \dot{h} = 0$.

A linear transformation is used to transform a relative state between the toroidal frame and rotating frame. A 6×1 relative Cartesian state vector that describes the state of the chaser spacecraft relative to the periodic orbit is defined as $\delta x = [\delta x, \delta y, \delta z, \delta \dot{x}, \delta \dot{y}, \delta \dot{z}]^T$. An equivalent relative state vector is defined using the nonsingular coordinates and coordinate rates as $\zeta = [\alpha, \beta, h, \dot{\alpha}, \dot{\beta}, \dot{h}]^T$. A 6×6 transformation matrix, T , that maps a state vector formulated in the toroidal coordinates frame to a state vector formulated in the rotating frame is defined as

$$T = \begin{bmatrix} R & 0_3 \\ R' & R \end{bmatrix} \quad (5)$$

As the matrices \mathbf{R} and \mathbf{R}' are dependent on the current reference fixed point along the periodic orbit, the transformation matrix is also dependent on the current fixed point. The transformation from a relative state vector defined in the rotating frame, $\delta\mathbf{x}$, to a relative state in the toroidal coordinate frame, ζ , is then expressed as $\zeta = \mathbf{T}^{-1}\delta\mathbf{x}$. The transformation matrix is full-rank and invertible so long as the associated oscillatory mode is not rectilinear in the rotating frame.

Transitioning Center Eigenspace Information to an Ephemeris Model

The complex eigenvector of the monodromy matrix of a periodic orbit is used to formulate the presented control strategy. Within the CR3BP, this eigenvector is numerically integrated along with the state along the periodic orbit and state of a chaser spacecraft. For application of the control strategy in the CR3BP, this implementation allows eigenvector information to be exactly specified at any time. However, to use toroidal coordinates within the ephemeris model an approximation of the complex eigenvector of the periodic orbit used as an initial guess for the reference trajectory is constructed using a cubic spline interpolation. Capturing the eigenvector information within a cubic spline interpolation allows the complex eigenvector to be evaluated from a piecewise polynomial and does not require additional numerical integration once generated. To compute the cubic spline approximation of the complex eigenvector, the 6×1 eigenvector is first numerically integrated in the CR3BP for one period then sampled evenly over time. The eigenvector is then evaluated at several fixed points, evenly distributed in time along the periodic orbit, to construct the cubic spline piecewise polynomial. In this implementation, the eigenvector is evaluated at 100 fixed points. Using this number of evaluations, the error between the interpolated eigenvector and true eigenvector in the CR3BP, defined as $\int_{t_0}^{t_0+T} |\mathbf{w}(t)_{\text{true}} - \mathbf{w}(t)_{\text{spline}}| dt$ using nondimensional units, is 7.784×10^{-7} . The cubic spline interpolation constructed using 100 evaluations across the periodic orbit is observed to be sufficient for the simulations in the following analysis.

Another consideration for the use of the complex eigenvector in the ephemeris model is that the continuous reference trajectory recovered in the ephemeris model to resemble a periodic orbit is not exactly periodic in the rotating frame of the Sun and Earth. To account for this, the cubic spline approximation of the eigenvector is redistributed over time for each revolution of the orbit. A revolution of the reference orbit is defined as two subsequent crossings of the xz plane with positive \dot{y} in the Sun-Earth barycentric, rotating coordinate system. To account for the variation in the time between crossings of each revolution, the time since crossing this plane, normalized by the time between crossing of the current revolution, is used to sample the cubic spline interpolation and return the appropriate eigenvector state. Additionally, after each revolution the complex eigenvector must be updated by the complex eigenvalue, λ . The eigenvector must be updated because of the natural quasi-periodic evolution of the eigenvector after a period of the periodic orbit, expressed by the eigenvalue relation: $\Phi(t+T, t)\lambda = \mathbf{w}(t)\lambda$. This is implemented by multiplying all eigenvector values in the interpolation by the complex eigenvalue during the eigenvector update each revolution. These steps enable the complex eigenvector, and thus the toroidal coordinates, to be sufficiently approximated in the ephemeris model for use with the presented control strategy. Future investigations of alternative methods for the transition of the complex eigenvector into the ephemeris model may provide benefits over the implemented strategy.

FORMATION STATION-KEEPING CONTROL STRATEGY

The local toroidal coordinates are leveraged to produce an impulsive feedback control strategy that enables multiple spacecraft using the same control law independently to track different ref-

erences on a center eigenspace of a periodic orbit. This strategy determines successive impulsive changes in velocity, $\Delta \mathbf{v}$, applied at a specified maneuver frequency. The strategy is formulated using insight from previously derived targeting strategies that require an STM to be computed between subsequent maneuver times.¹² However, a beneficial characteristic of this strategy is the ultimate removal of the requirement to compute the STM between maneuver epochs, resulting in a straightforward control strategy that is relatively computationally inexpensive.

Control Strategy Derivation

To derive the control strategy, the STM evaluated along the periodic orbit in the CR3BP between two subsequent maneuver times is first formulated in the toroidal coordinate frame. Consider the STM between time t_0 and t formulated in the rotating frame, $\Phi(t, t_0)$. The transformation matrix between the rotating and toroidal frame, \mathbf{T} , evaluated at times t_0 and t , is used to reformulate this STM into the toroidal coordinate frame, denoted ${}^Z\Phi(t, t_0)$. This transformation is expressed as ${}^Z\Phi(t, t_0) = \mathbf{T}(t)^{-1}\Phi(t, t_0)\mathbf{T}(t_0)$. The formulation of the STM in the toroidal coordinate frame describes the first-order mapping of initial and final deviations from the periodic orbit, defined using the toroidal coordinate relative state vector, ζ , expressed as ${}^Z\Phi(t, t_0) = \partial\zeta/\partial\zeta_0$.

The STM expressed in the toroidal frame is used to formulate a linear targeting scheme, which determines the impulsive maneuver required to reach a desired deviation from the periodic orbit after a specified time in a linearized dynamical model. Similar to previously derived linear targeting schemes formulated in the rotating frame,^{12,23} to calculate the required impulsive maneuver, the STM is decomposed into four quadrants. The quadrants of the STM formulated in the toroidal coordinate frame are labeled as

$${}^Z\Phi(t, t_0) = \begin{bmatrix} {}^Z\Phi_{11} & {}^Z\Phi_{12} \\ {}^Z\Phi_{21} & {}^Z\Phi_{22} \end{bmatrix} \quad (6)$$

Using these quadrant definitions, the first-order relation between the initial and final relative states defined using nonsingular toroidal coordinates is expressed as

$$\begin{bmatrix} z \\ z_{z'} \end{bmatrix} = \begin{bmatrix} {}^Z\Phi_{11} & {}^Z\Phi_{12} \\ {}^Z\Phi_{21} & {}^Z\Phi_{22} \end{bmatrix} \begin{bmatrix} z_0 \\ z_{z'_0} + \Delta z'_{z'_0} \end{bmatrix} \quad (7)$$

where $\Delta z'_{z'_0}$ is an instantaneous change in toroidal coordinate rates at t_0 corresponding to an impulsive maneuver. This instantaneous change in the coordinate rate relates to an instantaneous change in Cartesian velocity, $\Delta \mathbf{v}_0$, as $\Delta z'_{z'_0} = \mathbf{R}(t_0)^{-1}\Delta \mathbf{v}_0$. This expression is derived by calculating the partial derivative of Eq. (4) with respect to $\delta \mathbf{v}$.

At this step, the control strategy is formulated by assuming that the desired motion of the chaser spacecraft lies in the center eigenspace. Because motion within the center eigenspace in the linearized dynamical model is time-invariant when expressed in toroidal coordinates, the desired relative configuration is described by a constant description, z_d . Rearranging Eq. (7) and incorporating the relationship between $\Delta z'_{z'_0}$ and $\Delta \mathbf{v}_0$, the required change in Cartesian velocity required to reach the desired final configuration in linearized dynamics is

$$\Delta \mathbf{v}_0 = \mathbf{R}(t_0) \left({}^Z\Phi_{12}^{-1} (z_d - {}^Z\Phi_{11} z_0) - {}^Z z'_{z'_0} \right) \quad (8)$$

Note that only the upper quadrants of the STM are required. In this formulation, the $\Delta \mathbf{v}$ determined by Eq. (8) is confirmed to be equivalent to the maneuver determined by a Cartesian linear targeting

scheme using initial and final conditions converted from toroidal coordinates to relative Cartesian deviations.

The characteristics of the STM formulated in the toroidal coordinate frame enable approximations of the quadrants of the STM within the computation of an impulsive control maneuver. Because a relative toroidal state vector described by only nonzero values of α and β is constant over time in the linearized dynamical model, the upper-left quadrant of the STM expressed in the toroidal frame possesses the form

$${}^z\Phi_{11} = \frac{\partial z}{\partial z_0} = \begin{bmatrix} 1 & 0 & * \\ 0 & 1 & * \\ 0 & 0 & * \end{bmatrix} \quad (9)$$

To leverage this property, consider the first two terms of the Taylor series expansion of an STM, $\Phi(t, t_0)$, at t_0 ⁴⁰

$$\Phi(t, t_0) \approx \mathbf{I}_6 + \mathbf{A}(t_0)\delta t = \begin{bmatrix} \mathbf{I}_3 & \mathbf{0}_3 \\ \mathbf{0}_3 & \mathbf{I}_3 \end{bmatrix} + \begin{bmatrix} \mathbf{0}_3 & \mathbf{I}_3 \\ \mathbf{A}_3(t_0) & \mathbf{A}_4(t_0) \end{bmatrix} \delta t \quad (10)$$

where $\delta t = t - t_0$. Using these terms of the Taylor series expansion to approximate the STM formulated in the toroidal coordinate frame, the upper-left quadrant of the STM is approximated as ${}^z\Phi_{11} \approx \mathbf{I}_3$, and the upper-right quadrant is approximated as ${}^z\Phi_{12} \approx \delta t \mathbf{I}_3$. Thus, the upper-left quadrant of STM formulated in the toroidal frame shares two columns with the approximation of the quadrant.

Applying the approximation of the quadrants of the STM formulated in the toroidal coordinate frame within the targeting control law, a straightforward control strategy is developed. Substituting the approximated definitions of ${}^z\Phi_{11}$ and ${}^z\Phi_{12}$, the resulting impulsive control maneuver is determined as

$$\Delta v_0 = -\mathbf{R}(t_0) \left(\frac{z_0 - z_d}{\delta t} + {}^z z'_0 \right) \quad (11)$$

When the chaser spacecraft lies near the center eigenspace, h , and all three coordinate rates have near-zero values, minimizing the impact of the differences between the true and approximated values of ${}^z\Phi_{12}$ and the third column of ${}^z\Phi_{11}$. In fact, when the chaser spacecraft lies exactly within the center eigenspace, indicated by $h = \dot{\alpha} = \dot{\beta} = \dot{h} = 0$, the Δv_0 determined by Eq. (8) and Eq. (11) are equivalent. Ultimately, the simplifications remove the computation of the STM between successive maneuvers while enabling station-keeping of specified deviations from a reference trajectory in the CR3BP and ephemeris models.

Station-Keeping Performance in the CR3BP

The simplifications to the STM formulated in the toroidal coordinate frame are evaluated in the CR3BP. Using the Sun-Earth southern L_1 halo orbit defined previously as the formation center, a maneuver interval of 10 maneuvers per revolution is selected, corresponding to a time between maneuvers of approximately $\delta t = 17.8$ days, or $\delta t = 0.30598$ in nondimensional units of time. Starting from apogee, the nondimensionalized upper quadrants of the STM formulated in the toroidal frame evaluated along the periodic orbit for δt are equal to

$${}^z\Phi_{11} = \begin{bmatrix} 1 & 0 & 0.04346 \\ 0 & 1 & -0.04859 \\ 0 & 0 & 1.3121 \end{bmatrix} \quad {}^z\Phi_{12} = \begin{bmatrix} 0.33730 & -0.032148 & 0.000263 \\ 0.032464 & 0.33727 & -0.010084 \\ 0.006635 & 0.003438 & 0.33693 \end{bmatrix}$$

The form of ${}^z\Phi_{11}$ is consistent with the form of Eq. (9). Furthermore, the diagonal terms of ${}^z\Phi_{12}$ possess values near the nondimensional value of δt and smaller off-diagonal terms. As the time between successive maneuvers decreases, the approximations of the STM quadrants better represent the true STM quadrants.

These approximations are further assessed by comparing the performance of the impulsive control strategy formulated using the true approximated STM. The strategies are applied to the control of a single chaser spacecraft relative to the Sun-Earth L_1 halo orbit. The desired relative trajectory is located on the surface of a first-order approximation of an invariant torus, described by a constant state vector of $\zeta_d = [1000, 0, 0, 0, 0, 0]^T$ (km, km/s) and is constant. The initial relative state of the chaser spacecraft is slightly perturbed from the desired relative state, defined as $\zeta = [1000, 0, 10, 0, 0, 0]^T$ (km, km/s) relative to apogee. The control strategy is then applied using the impulsive maneuvers determined using the true STM, as described in Eq. (8), and the approximated STM, described in Eq. (11), for a maneuver interval of 10 maneuvers per revolution. Each controlled trajectory is propagated from the initial conditions for five revolutions of the halo orbit. The error of each trajectory, defined as the magnitude of the Cartesian position difference between the spacecraft and the desired trajectory, is plotted over time, normalized by the period, in Figure 4. The error of the trajectory associated with maneuvers determined using the full STM is depicted in blue, while the error associated with the approximated STM is depicted in red. While using the true STM results in lower average error over time, maximum steady-state error is similar between the two control formulations, at approximately 0.5 km or 0.05% of α_d . The trajectory associated with the approximated STM also exhibits a slower convergence to the steady-state error compared to the trajectory associated to the true STM. This example demonstrates that the impulsive control strategy leveraging the approximated quadrants of the STM supports a chaser spacecraft station-keeping near the L_1 halo orbit in the Sun-Earth CR3BP.

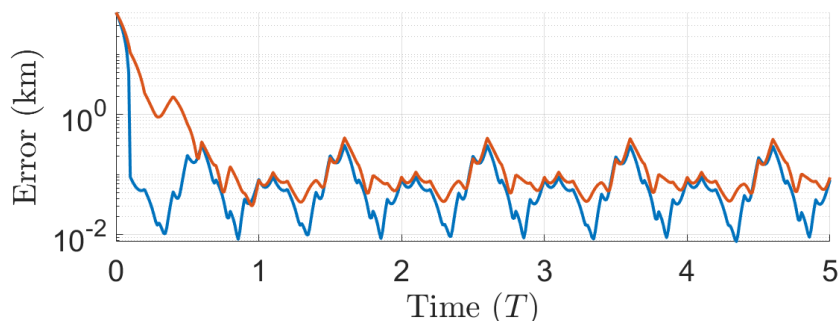


Figure 4. Relative error over time for the impulsive control strategy using the STM (blue) and the approximated STM (red).

The performance of the control strategy with the simplified STM is assessed at different separation distances and maneuver intervals to demonstrate the control strategy in multiple scenarios. Values of the desired size of the torus, described by ε_d , near the Sun-Earth L_1 halo orbit are selected from between 0 and 1000 km. The desired angle coordinate is kept constant at $\theta_d = 0$ rad. The time between subsequent maneuvers is defined using the number of maneuvers per revolution, N , and is varied between $N = 1$ and 30. For each simulation, the controlled trajectory is initialized on the desired state relative to apogee of the reference orbit and propagated for five periods. The maximum position error is defined as the maximum magnitude of the Cartesian position difference

between the spacecraft and the desired trajectory over the five periods. Two-dimensional plots of cumulative Δv and maximum position error over time as a function of ε_d and N are displayed in Figure 5(a) and Figure 5(b), respectively. Over the propagation duration, divergence of the station-keeping spacecraft is defined to occur if the position error between the spacecraft's position and desired position is greater than 0.1% of ε_d and also greater than one meter. Divergence is represented in Figures 5(a) and 5(b) as blank areas. When less than six maneuvers are applied per orbit, the control trajectory is observed to diverge from the reference. However, for $N \geq 8$, long-term bounded motion is observed for all values of ε_d . As the number of impulsive maneuvers per orbit increases beyond $N = 8$, the cumulative Δv is observed to decrease slowly, while maximum position error over time steadily decreases as maneuver frequency increases. Note that required Δv per orbit is small, on the order of magnitude of mm/s.

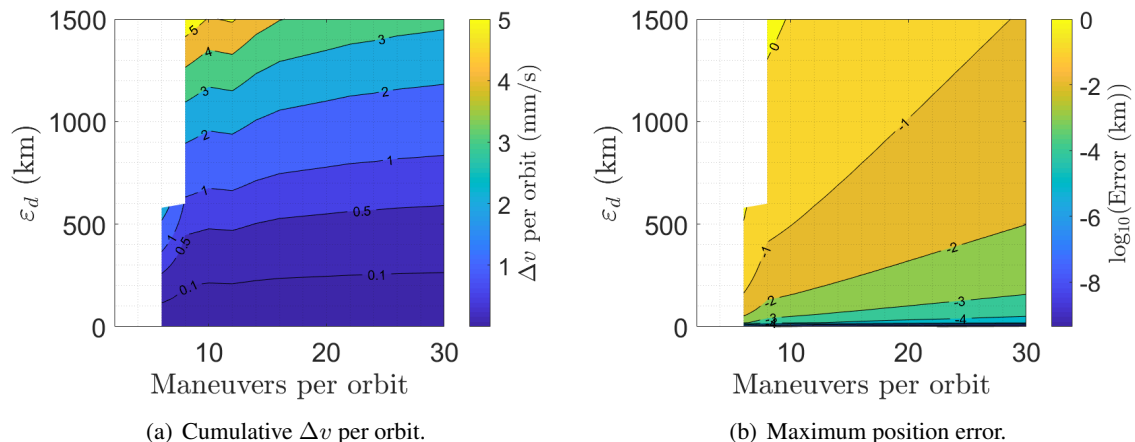


Figure 5. Performance of the simplified station-keeping controller near an unstable Sun-Earth L_1 southern halo orbit in the CR3BP.

Three controlled trajectories are examined individually to compare the performance of the strategy in the CR3BP using different values of N . The selected trajectories each correspond to a desired relative state of $\zeta_d = [1000, 0, 0, 0, 0, 0]^T$ (km, km/s) while the maneuver frequencies are compared for $N = 5, 10, 30$. The position error versus time is plotted in Figure 6(a) for each of the three trajectories. The cumulative Δv required by the control strategy for each trajectory is plotted versus time in Figure 6(b). At a maneuver frequency of $N = 5$, the controlled trajectory is observed to diverge from the desired reference, consistent with the divergent regions in Figure 5. However, at $N = 10$ and $N = 30$, the associated controlled responses are observed to remain bounded to the desired reference. Comparing the trajectories corresponding to $N = 10$ and $N = 30$, increasing the number of maneuvers per orbit is observed to lower the average position error and reduce the required Δv . If a low number of maneuvers per revolution is desired (e.g., $N = 5$), the true STM may be used to produce bounded motion. However, this analysis demonstrates that the full STM is not required for producing bounded relative motion near the center eigenspace of a periodic orbit in the CR3BP. Of course, applying the control strategy near different periodic orbits will produce different responses, motivating future assessments of the control strategy near different reference orbits in the CR3BP.

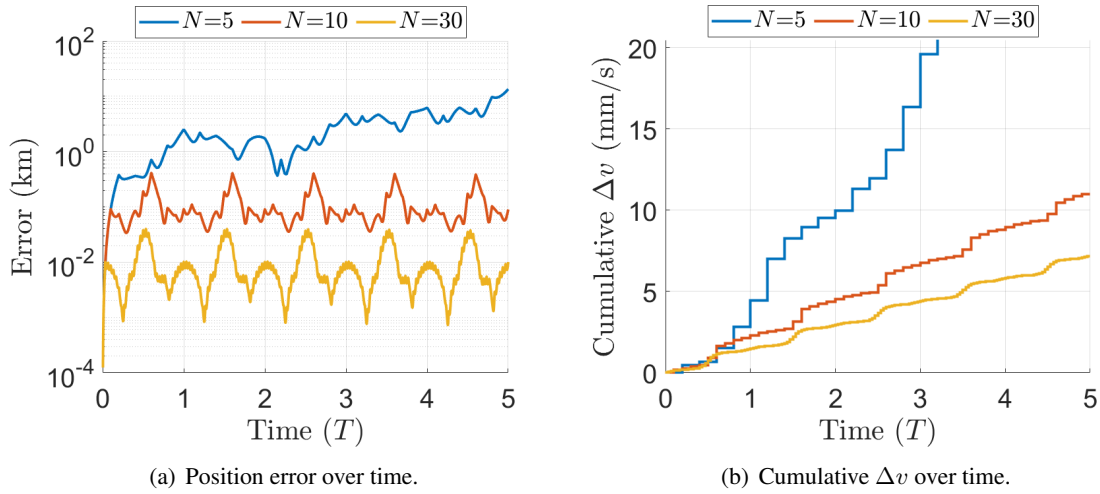


Figure 6. Position error and cumulative Δv over time for different maneuver frequencies applied in the Sun-Earth CR3BP.

Station-Keeping in the Ephemeris Model

To assess the performance of the presented control strategy in a higher-fidelity simulation, a Monte Carlo analysis of the control strategy is conducted in the ephemeris model. Compared to the Sun-Earth CR3BP, the higher-fidelity ephemeris model considers ephemeris positions of the Sun and Earth, the gravity of the Moon, as well as acceleration due to SRP. To further increase fidelity, navigational errors and thruster firing errors are also considered, with 3σ values selected based on historical and theorized values for spacecraft operating near the Sun-Earth L_1 and L_2 equilibrium points.^{37,41} Injection errors are defined as the initial deviation of the chaser spacecraft from the desired trajectory error. Navigational errors are added to chaser spacecraft state within the determination of the required impulsive maneuver to simulate state estimation. Finally, thruster firing errors are defined as a magnitude percentage error of the implemented maneuver; however, thruster pointing errors are not simulated. To assess the performance of the control strategy, Monte Carlo simulations are conducted to average the results of 100 trials of the strategy applied using $N = 10, 15, 30$. The parameters of the Monte Carlo simulations are summarized in Table 1. For each simulation, the chaser spacecraft is initialized relative to the initial state of the reference trajectory at the southern crossing of the xz plane, approximately at apogee. Each controlled trajectory is then propagated for 10 revolutions in the rotating frame, approximately 1777.4 days or 4.86 years.

Table 1. Monte Carlo simulation parameters in the ephemeris model.

Parameter	Value
Initial epoch	Jan. 1, 2025
Propagation duration	1777.4 days
Desired configuration	$\mathbf{z}_d = [1000 \text{ km}, 0 \text{ km}, 0 \text{ km}]^T$
Navigation and injection position error	$3\sigma_r = 10 \text{ km}$
Navigation and injection velocity error	$3\sigma_v = 10 \text{ mm/s}$
Maneuver magnitude error	$3\sigma_{\Delta v} = 3\%$
Maneuvers per revolution	$N = 10, 15, 20$

In the Monte Carlo simulations of the control of the chaser spacecraft in the ephemeris model, the control strategy maintains motion bounded to the reference trajectory for reasonable Δv . The control usage requirements and position error results averaged over the 100 trials of the Monte Carlo simulations are summarized in Table 2. For each maneuver frequency, the Δv requirements are less than 1 m/s per revolution. However, in contrast to the assessment the CR3BP, increasing the number of maneuvers per revolution instead results in an increase in the total Δv required. Increasing the number of maneuvers per revolution is observed to reduce the average and maximum position error.

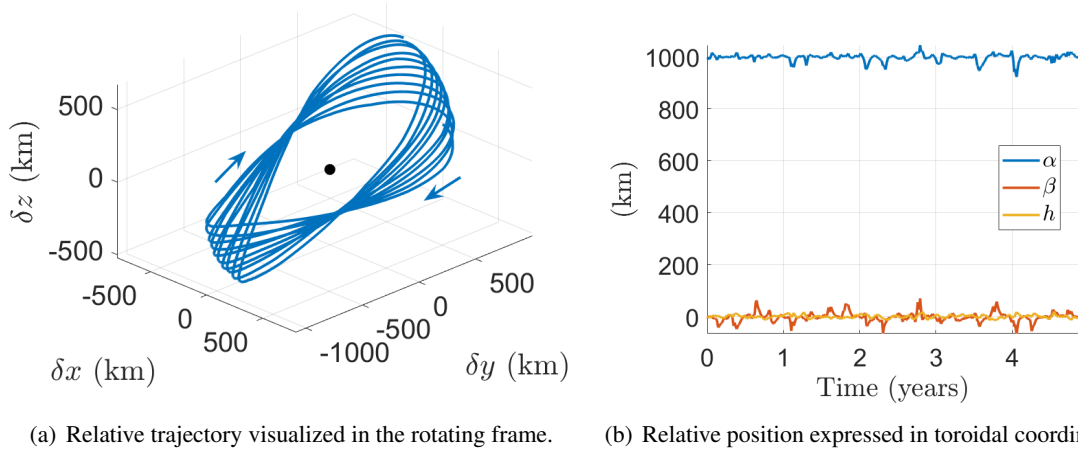
Table 2. Monte Carlo results of the control strategy for ten revolutions of the reference trajectory.

Maneuvers per revolution	10	15	20
Min of total Δv (m/s)	2.566	3.412	4.856
Mean of total Δv (m/s)	2.945	2.891	5.427
Max of total Δv (m/s)	3.330	4.455	5.936
Mean of max error (km)	78.793	44.849	33.150
Max of max error (km)	126.15	67.733	51.053

A single simulation trajectory from the Monte Carlo analysis is analyzed in more detail. Plots associated with the controlled trajectory applying the presented control strategy at a maneuver frequency of $N = 15$ are included in Figure 7. The controlled trajectory of the chaser spacecraft is plotted in Figure 7(a) in the Sun-Earth rotating frame relative to the reference trajectory, indicated by a black marker. Oscillatory bounded motion relative to the reference trajectory is observed, with no secular drift towards or away from the reference orbit. The corresponding position of this trajectory is plotted in Figure 7(b) using toroidal coordinates. The desired configuration is constant over time, and the controlled configuration of the chaser spacecraft in the ephemeris is observed to remain close to the nominal values. The Monte Carlo analysis and sampled trajectory demonstrate the control strategy supports a chaser station-keeping to a specified deviation located on the surface on an approximated invariant torus relative to the reference trajectory in the ephemeris model. Of course, modification of the error parameters, dynamical model, or spacecraft properties may impact results.

APPLICATION TO A CONCEPTUAL SPACECRAFT FORMATION

The presented control strategy is applied to the control of a conceptual spacecraft formation consisting of six spacecraft near Sun-Earth L_1 . The conceptual scenario consists of six spacecraft located at six distinctive locations on an invariant curve centered at the reference trajectory. This simulation considers the formation post-injection, where the spacecraft are assumed to instantaneously begin applying the control strategy. The objective of the control of the formation is to prevent spacecraft drifting towards each other while leveraging natural bounded relative motion near the periodic orbit to reduce control usage costs. The six spacecraft each apply the control strategy to station-keep near their respective desired trajectories, which are evenly distributed along the invariant curve. Each spacecraft applies the control strategy independently, without state knowledge of the other spacecraft in the formation. Each spacecraft applies impulsive maneuvers determined by Eq. (11) at a maneuver frequency of $N = 10$ maneuvers per revolution of the halo orbit in the rotating frame, or approximately 18 days between maneuvers. For this example, the maneuvers of the six spacecraft are synchronized to occur simultaneously; however, this synchronization is not



(a) Relative trajectory visualized in the rotating frame. (b) Relative position expressed in toroidal coordinates.

Figure 7. Example relative trajectory of a chaser spacecraft in the ephemeris model applying the impulsive control strategy using 15 maneuvers per revolution.

a requirement of the control strategy. Injection, navigation, and maneuver magnitude 3σ values are consistent with the values listed in Table 1. The controlled trajectories are propagated in the ephemeris model for 10 revolutions of the reference orbit, or approximately five years.

The configuration of the formation over time applying the presented control strategy is analyzed, leveraging the insight gained from the toroidal coordinate frame. The trajectories of each spacecraft in the formation are visualized in the Sun-Earth rotating frame relative to the reference orbit in Figure 8(a). Within the Cartesian rotating frame, the formation is observed to stay bounded to the vicinity of the reference trajectory, located at the origin. The maximum magnitude of the Cartesian position error difference from the desired trajectory over time is observed to be less than 110 km for each spacecraft. However, the same six trajectories are visualized in the nonsingular toroidal coordinate frame relative to the reference trajectory in Figure 8(b). In the nonsingular toroidal coordinate frame, the first-order approximation of the invariant curve is represented as a time-invariant circle centered at the reference trajectory that spans the $\alpha\beta$ plane with a radius of 1000 km. This first-order invariant curve, which is represented as an ellipse in a Cartesian reference frame, is circular in the toroidal reference frame because of the time-varying magnitudes of the basis vectors, \mathbf{r}_r and \mathbf{r}_i , of the reference frame. The trajectories of controlled spacecraft are observed to remain near this circle, centered at their individual deviations from the reference trajectory. Each of trajectories also exhibits small values of the out-of-plane coordinate, h , that are much smaller than α and β , with no secular drift observed.

Finally, the Δv requirements of the spacecraft formation in the ephemeris model are assessed. The maneuver magnitude of each impulsive maneuver for each of the six spacecraft are plotted versus time in Figure 9(a) while the cumulative Δv usage is plotted in Figure 9(b), with coloring consistent with Figure 8. The magnitude per each maneuver is observed to be similar to previously developed station-keeping algorithms applied to spacecraft near Sun-Earth halo orbits,⁴² and the required Δv of less than 1 m/s/year is comparable to the station-keeping requirements of previously flown missions near SE L_1 .²² Possible future investigations include modifications to the control strategy formulation to reduce overall Δv or the required number of maneuvers per revolution.

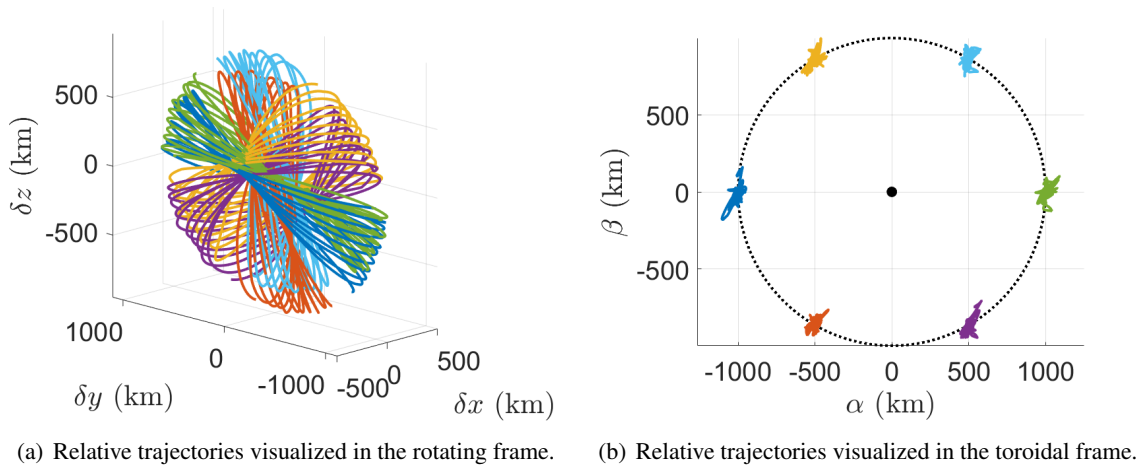


Figure 8. Relative trajectories of the six spacecraft formation station-keeping near the SE L_1 reference orbit in the ephemeris model.

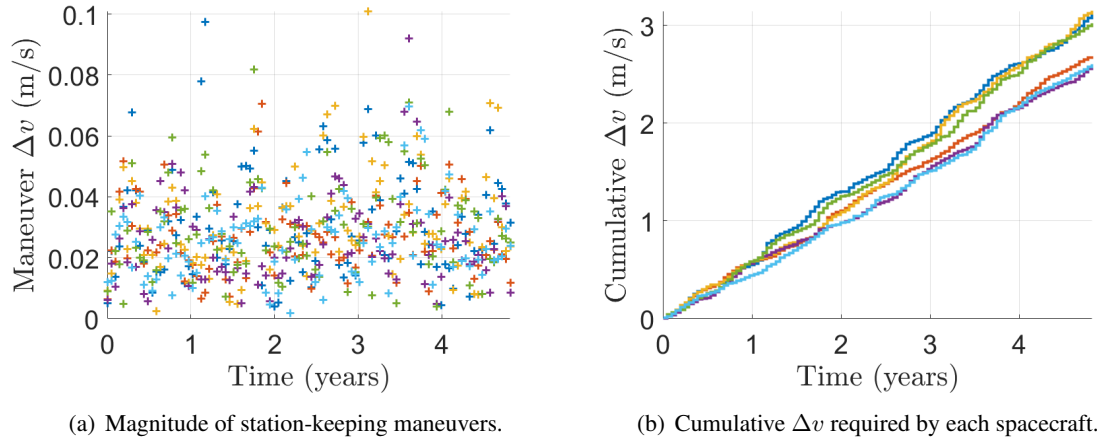


Figure 9. Station-keeping control individual maneuver magnitudes and cumulative Δv requirements for the six spacecraft formation.

CONCLUSION

A control strategy for spacecraft formations near a periodic orbit in a multi-body system is developed using insight into the center eigenspace of the periodic orbit. The strategy enables multiple spacecraft to independently apply impulsive maneuvers to maintain in a desired configuration using the center eigenspace as a natural reference input. A formulation of local toroidal coordinates for describing motion on a center eigenspace is used to formulate the control strategy. The properties of this state representation enable the presented control strategy to perform similarly to a targeting strategy without a requirement to compute a state transition matrix between maneuvers. The control strategy is evaluated in the Sun-Earth CR3BP and a point-mass ephemeris model of the Sun-Earth-Moon system with perturbations from solar radiation pressure. Finally, the strategy is applied to a conceptual distributed spacecraft mission near a Sun-Earth L_1 halo orbit to demonstrate the utility of the control strategy and local toroidal coordinates in higher-fidelity mission design. As distributed

spacecraft architectures become more prevalent in the near-future, this work continues to support the potential for application of dynamical systems theory in the CR3BP to formation control strategies.

ACKNOWLEDGMENTS

This work was supported by a Graduate Assistance in Areas of National Need Fellowship from the Smead Aerospace Engineering Sciences Department at the University of Colorado Boulder.

REFERENCES

- [1] J. Le Moigne, “Distributed Spacecraft Missions (DSM) Technology Development at NASA Goddard Space Flight Center,” *Institute of Electrical and Electronics Engineers International Geoscience and Remote Sensing Symposium*, 2018, pp. 293–296, <https://doi.org/10.1109/IGARSS.2018.8519065>.
- [2] C. Beichman, G. Gómez, M. Lo, J. Masdemont, and L. Romans, “Searching for Life with the Terrestrial Planet Finder: Lagrange Point Options for a Formation Flying Interferometer,” *Advances in Space Research*, Vol. 34, No. 3, 2004, pp. 637–644, <https://doi.org/10.1016/j.asr.2003.05.032>.
- [3] K. G. Carpenter, C. J. Schrijver, M. Karovska, and S. V. M. Team, “The Stellar Imager (SI)-A Mission to Resolve Stellar Surfaces, Interiors, and Magnetic Activity,” *Astronomical Society of the Pacific*, Vol. 412, 2009, p. 91.
- [4] C. V. M. Fridlund, “Darwin - The Infrared Space Interferometry Mission,” Aug. 2000. European Space Agency Bulletin.
- [5] J. Gardner, J. Mather, M. Clampin, R. Doyon, M. Greenhouse, H. Hammel, J. Hutchings, P. Jakobsen, S. Lilly, K. Long, J. Lunine, M. McCaughrean, M. Mountain, J. Nella, G. Rieke, M. Rieke, H.-W. Rix, E. Smith, G. Sonneborn, and G. Wright, “The James Webb Space Telescope,” *Space Science Reviews*, Vol. 123, 2009, pp. 485–606, <https://doi.org/10.1007/s11214-006-8315-7>.
- [6] J. Stuart, A. Dorsey, F. Alibay, and N. Filipe, “Formation Flying and Position Determination for a Space-Based Interferometer in GEO Graveyard Orbit,” *Institute of Electrical and Electronics Engineers Aerospace Conference*, 2017, pp. 1–19, <https://doi.org/10.1109/AERO.2017.7943705>.
- [7] J. Kasper, J. Lazio, A. Romero-Wolf, J. Lux, and T. Neilsen, “The Sun Radio Interferometer Space Experiment (SunRISE) Mission Concept,” *Institute of Electrical and Electronics Engineers Aerospace Conference*, 2019, pp. 1–11, <https://doi.org/10.1109/AERO.2019.8742146>.
- [8] M. W. Lo, “Satellite-Constellation Design,” *Computing in Science and Engineering*, Vol. 1, 1999, pp. 58–67, <https://doi.org/10.1109/5992.743623>.
- [9] Z. P. Olikara and D. J. Scheeres, “Numerical Methods for Computing Quasi-Periodic Orbits and their Stability in the Restricted Three-Body Problem,” *International Academy of Astronautics Conference on Dynamics and Control of Space Systems*, 2012, pp. 911–930.
- [10] E. Kolumen, N. Kasdin, and P. Gurfil, “Multiple Poincaré Sections Method for Finding the Quasiperiodic Orbits of the Restricted Three Body Problem,” *Celestial Mechanics and Dynamical Astronomy*, Vol. 112, 10 2012, pp. 47–74, <https://doi.org/10.1007/s10569-011-9383-x>.
- [11] B. T. Barden and K. C. Howell, “Dynamical Issues Associated with Relative Configurations of Multiple Spacecraft Near the Sun-Earth/Moon L1 Point,” *AAS/AIAA Astrodynamics Specialist Conference*, 1999.
- [12] K. C. Howell and B. T. Barden, “Trajectory Design and Stationkeeping for Multiple Spacecraft in Formation Near the Sun-Earth L1 Point,” *IAF 50th International Astronautical Congress.*, 1999.
- [13] B. G. Marchand and K. C. Howell, “Control Strategies for Formation Flight in the Vicinity of the Libration Points,” *Journal of Guidance, Control, and Dynamics*, Vol. 28, No. 6, 2005, pp. 1210–1219, <https://doi.org/10.2514/1.11016>.
- [14] K. C. Howell and B. G. Marchand, “Natural and Non-Natural Spacecraft Formations Near the L1 and L2 Libration Points in the Sun–Earth/Moon Ephemeris System,” *Dynamical Systems*, Vol. 20, No. 1, 2005, pp. 149–173, <https://doi.org/10.1080/1468936042000298224>.
- [15] C. Simó, G. Gómez, J. Llibre, R. Martínez, and J. Rodríguez, “On the Optimal Station Keeping Control of Halo Orbits,” *Acta Astronautica*, Vol. 15, No. 6-7, 1987, pp. 391–397, [https://doi.org/10.1016/0094-5765\(87\)90175-5](https://doi.org/10.1016/0094-5765(87)90175-5).
- [16] T. Pavlak and K. C. Howell, “Strategy for Optimal, Long-Term Stationkeeping of Libration Point Orbits in the Earth-Moon System,” *AIAA/AAS Astrodynamics Specialist Conference*, 2012.
- [17] W. Wiesel and W. Shelton, “Modal Control of an Unstable Periodic Orbit,” *Journal of the Astronautical Sciences*, 1983.

- [18] L. Millard and K. C. Howell, "Optimal Reconfiguration Maneuvers for Spacecraft Imaging Arrays in Multi-Body Regimes," *Acta Astronautica*, Vol. 63, 12 2008, pp. 1283–1298, <https://doi.org/10.1016/j.actaastro.2008.05.016>.
- [19] I. Elliott and N. Bosanac, "Spacecraft Formation Control Near a Periodic Orbit Using Geometric Relative Coordinates," *AAS/AIAA Spaceflight Mechanics Meeting*, 2021.
- [20] D. J. Scheeres, F.-Y. Hsiao, and N. X. Vinh, "Stabilizing Motion Relative to an Unstable Orbit: Applications to Spacecraft Formation Flight," *Journal of Guidance, Control, and Dynamics*, Vol. 26, No. 1, 2003, pp. 62–73, <https://doi.org/10.2514/2.5015>.
- [21] D. Folta, T. Pavlak, K. C. Howell, M. Woodard, and D. Woodfork, "Stationkeeping of Lissajous Trajectories in the Earth-Moon System with Applications to ARTEMIS," *Advances in the Astronautical Sciences*, 2010.
- [22] M. Shirobokov, S. Trofimov, and M. Ovchinnikov, "Survey of Station-Keeping Techniques for Libration Point Orbits," *Journal of Guidance, Control, and Dynamics*, Vol. 40, No. 5, 2017, pp. 1085–1105, <https://doi.org/10.2514/1.G001850>.
- [23] R. Qi, S. Xu, and M. Xu, "Impulsive Control for Formation Flight about Libration Points," *Journal of Guidance, Control, and Dynamics*, Vol. 35, No. 2, 2012, pp. 484–496, <https://doi.org/10.2514/1.54383>.
- [24] K. C. Howell and H. J. Pernicka, "Station-Keeping Method for Libration Point Trajectories," *Journal of Guidance, Control, and Dynamics*, Vol. 16, No. 1, 1993, pp. 151–159, <https://doi.org/10.2514/3.11440>.
- [25] K. C. Howell and S. Gordon, "Orbit Determination Error Analysis and a Station-Keeping Strategy for Sun-Earth L1 Libration Point Orbits," *Journal of The Astronautical Sciences*, Vol. 42, 1994, pp. 207–228.
- [26] I. Elliott and N. Bosanac, "Geometric Relative Orbital Element Set for Motion Near a Periodic Orbit with Oscillatory Modes," *AAS/AIAA Astrodynamics Specialist Conference*, 2020.
- [27] V. Szebehely, *Theory of Orbits*. Academic Press, 1967.
- [28] W. S. Koon, M. W. Lo, J. E. Marsden, and S. D. Ross, *Dynamical Systems, the Three-Body Problem and Space Mission Design*. Marsden Books, 2006.
- [29] NASA Navigation and Ancillary Information Facility, "SPICE Toolkit," <https://naif.jpl.nasa.gov/naif/aboutspice.html>. Accessed December 2020.
- [30] J. O. Cappellari, C. E. Vélez, and A. J. Fuchs, *Mathematical Theory of the Goddard Trajectory Determination System: Chapter 4, Perturbation Models and Variational Equations*, pp. 4.60–4.62. Goddard Space Flight Center, 1976.
- [31] D. A. Vallado and W. D. McClain, *Fundamentals of Astrodynamics and Applications*. Space Technology Library, Microcosm Press, 2001.
- [32] S. P. Hughes, "General Mission Analysis Tool (GMAT)," *International Conference on Astrodynamics Tools and Techniques (ICATT)*, 2016.
- [33] A. Farres, C. Webster, and D. Folta, "High Fidelity Modeling of SRP and its Effect on the Relative Motion of Starshade and WFIRST," *Space Flight Mechanics Meeting*, 2018, <https://doi.org/10.2514/6.2018-2227>.
- [34] A. Farres and J. Petersen, "Solar Radiation Pressure Effects on the Orbital Motion at SEL2 for the James Webb Space Telescope," *AAS/AIAA Astrodynamics Specialist Conference*, 2019.
- [35] J. R. Wertz, D. F. Everett, and J. J. Puschell, *Space Mission Engineering: The New SMAD*, ch. 25.3. Space Technology Library, Microcosm Press, 2011.
- [36] T. A. Pavlak, "Mission Design Applications in the Earth-Moon System: Transfer Trajectories and Stationkeeping," Masters Thesis, Purdue University, West Lafayette, IN, 2010.
- [37] D. W. Dunham and C. E. Roberts, "Stationkeeping Techniques for Libration-Point Satellites," *The Journal of the Astronautical Sciences*, Vol. 49, No. 1, 2001, pp. 127–144, <https://doi.org/10.1007/BF03546340>.
- [38] K. C. Howell, "Three-Dimensional, Periodic, 'Halo' Orbits," *Celestial Mechanics*, Vol. 32, No. 1, 1984, pp. 53–71.
- [39] R. A. Calico and W. E. Wiesel, "Control of Time-Periodic Systems," *Journal of Guidance, Control, and Dynamics*, Vol. 7, No. 6, 1984, pp. 671–676, <https://doi.org/10.2514/3.19911>.
- [40] L. Markley, "Approximate Cartesian State Transition Matrix," *The Journal of the Astronautical Sciences*, Vol. 34, No. 2, 1986, pp. 161–169.
- [41] B. Sease, J. Myers, J. Lorah, and C. Webster, "Preliminary Analysis of Ground-Based Orbit Determination Accuracy for the Wide Field Infrared Survey Telescope (WFIRST)," *AAS/AIAA Astrodynamics Specialist Conference*, 2017.
- [42] N. Bosanac, C. Webster, K. C. Howell, and D. C. Folta, "Trajectory Design for the Wide Field Infrared Survey Telescope Mission," *Journal of Guidance, Control, and Dynamics*, Vol. 42, No. 9, 2019, pp. 1899–1911, <https://doi.org/10.2514/1.G004179>.